Optical and Surface Structural Properties of Mn^{2+}-Doped ZnSe Nanoparticles

Thaddeus J. Norman, Jr., Donny Magana, Thea Wilson, Colin Burns, Jin Z. Zhang*

Department of Chemistry, University of California, Santa Cruz, California 95064

Daliang Cao, and Frank Bridges

Department of Physics, University of California, Santa Cruz, California 95064

Received: December 22, 2002; In Final Form: April 23, 2003

Mn^{2+}-doped ZnSe nanoparticles were synthesized from molecular cluster precursors. Four ZnSe nanoparticle samples, one with low Mn^{2+} concentration (A), one with an intermediate Mn^{2+} concentration (B), one with a high Mn^{2+} concentration (C), and one with no Mn^{2+}, were prepared and characterized using UV−vis, luminescence, electron spin resonance (ESR), and X-ray absorption fine structure (XAFS) techniques. The sample with no Mn^{2+} had a sharp ZnSe band edge emission peak and a quantum yield of ∼2%. The samples with Mn^{2+} had a significant decrease in band edge emission. Sample A had no Mn^{2+} $^4T_1 \rightarrow {}^6A_1$ emission but showed some ZnSe band edge emission and trap state emission. Sample B had Mn^{2+} $^4T_1 \rightarrow {}^6A_1$ emission and a further reduction in ZnSe band edge emission and trap state emission. Sample C showed an increase in the Mn^{2+} $^4T_1 \rightarrow {}^6A_1$ emission, a dramatic increase in trap state emission, and essentially no ZnSe band edge emission. The overall emission from all four samples was quenched with time. To better understand these observations, XAFS and ESR data were taken to characterize the local structural and chemical environment of the Mn^{2+} ions. The XAFS data indicated that there was a reduction in the Zn and Mn first neighbor Se coordination from the bulk value but a lack of a reduction in the Se first neighbor coordination. This suggests that the core of the nanoparticles resembles that of bulk ZnSe, and the surface of the particle has a higher concentration of metal atoms. We propose that the surface Mn^{2+} possessed an octahedral geometry due to significant OH^-/O^{2-} coordination and the interior Mn^{2+} occupied the Zn^{2+} tetrahedral site. The overall low Mn^{2+} emission quantum yield (>0.1%) is primarily due to the presence of Mn^{2+} on the particle surface, and the decrease in Mn^{2+} emission overtime is attributed to the quenching of the luminescence by OH^-/O^{2-} coordinated to the surface metal ions. In sample C, which had the highest Mn^{2+} concentration, the surface Mn^{2+} enhanced the disorder of the nanoparticle surface structure, resulting in an increase in trap state emission.

Introduction

Semiconductor nanomaterials have been studied extensively because of their potential application in electronic devices and the opportunity they offer to study the effects of quantum confinement.[1−14] A unique subset of semiconductor nanomaterials is doped semiconductor nanoparticles. Mn^{2+}-doped ZnS nanoparticles, commonly denoted ZnS:Mn, are one of the most studied doped nanoparticle systems.[15−30] It has been determined that the luminescence properties of ZnS:Mn nanoparticles are not significantly different from those of the bulk material, although the luminescence characteristics are dependent upon S^{2-} and Mn^{2+} concentration and structural properties of the nanoparticles.[16,17,23,24,27] The $^4T_1 \rightarrow {}^6A_1$ Mn^{2+} emission intensity generally increases with increasing Mn^{2+} concentration; however, quenching of Mn^{2+} emission has been observed at high Mn^{2+} concentrations.[25,28] The local environment around the Mn^{2+} in the nanoparticles has been studied using X-ray absorption fine structure (XAFS)[18,19] and electron spin resonance (ESR).[20,25,30] XAFS measurements assign the Mn^{2+} dopant to the tetrahedral Zn^{2+} site in the lattice. The ESR signal is typical of that of Mn^{2+} spins in a tetrahedral crystal field, indicating that the Mn^{2+} ion substitutes for Zn^{2+} in the lattice. An anomalous resonance has also been observed in the ESR spectrum of ZnS:Mn. This resonance has been attributed to a Mn^{2+} defect with octahedral symmetry.[25,30] The location of this defect site, whether it is on the surface of the particle or in the interior, has not been fully established. Mn^{2+}-doped CdS and Mn^{2+}-doped CdSe nanoparticles also display a similar ESR signature.[31−33] An etching study of Mn^{2+}-doped CdSe nanoparticles suggests that this defect site is a surface site. The ESR spectra of the samples with high Mn^{2+} concentration show signs of Mn−Mn spin interaction. This exchange interaction in ZnS:Mn could be related to the quenching of the luminescence at high Mn^{2+} concentrations.[25]

Mn^{2+}-doped ZnSe nanoparticles had not been studied until recently because of the synthetic challenge in making high quality ZnSe nanoparticles. Hines et al.[34] were the first to report the synthesis of highly luminescent monodisperse undoped ZnSe nanoparticles. This was achieved by changing the solvent of the popular TOP/TOPO method for nanoparticle synthesis from TOP/TOPO to TOP/hexadecylamine (HDA). Shortly afterward, Suyver et al.[35] and Norris et al.[36] demonstrated that the TOP/HDA method can be further modified to synthesize Mn^{2+}-doped ZnSe nanoparticles. Their results suggest that the Mn^{2+} ion incorporates primarily into the center of the nanoparticle and that the luminescence of the material is dependent upon the Mn^{2+} concentration in the particle. The presence of Mn^{2+} defect sites and their effect on the luminescence was not fully addressed.

* Corresponding author.

10.1021/jp027804g CCC: $25.00
Published on Web 06/10/2003

Cumberland et al.[37] also reported a synthesis for undoped ZnSe nanoparticles. In the synthesis, the molecular cluster $(Me_4N)_4[Zn_{10}Se_4(SPh)_{16}]$ was decomposed in HDA at high temperatures. This process led to the formation of monodisperse, highly luminescent ZnSe nanoparticles. This method of synthesis was adapted to prepare a variety of II−VI nanoparticles, including Co^{2+}-doped CdSe nanoparticles.[38] It was proposed that under the reaction conditions these $(Me_4N)_4[M_{10}Se_4(SPh)_{16}]$ clusters (M = metal) fragment to M_6Se_4 clusters. The HDA coordinates to the cluster fragments, preventing the precipitation of bulk semiconductor material and allowing for the controlled growth of nanoparticles. Another feature of these clusters is their ability to exchange metal and chalcogenide atoms among each other.[39] It was this property that was exploited in the synthesis of the Co^{2+}-doped CdSe nanoparticles.

In this paper, we demonstrate that the method of Cumberland et al. can be adapted to prepare Mn^{2+}-doped ZnSe nanoparticles. The nanoparticle synthesis was monitored using UV−vis and luminescence spectroscopy. Interestingly, Mn^{2+} emission was not observed until late in the reaction, and the presence of Mn^{2+} significantly quenched the ZnSe band edge emission. The amount of Mn^{2+} used in the synthesis was varied in order to qualitatively determine the effect of Mn^{2+} on the emission properties of the ZnSe nanoparticles. The amount of band edge, trap state, and Mn^{2+} $^4T_1 \rightarrow {}^6A_1$ emission was dependent on the amount of Mn^{2+} present in the reaction solution. XAFS and ESR measurements were performed on the Mn^{2+}-doped ZnSe nanoparticles and the initial precursor clusters to determine how the structure and chemical environment relate to observed luminescence properties. These measurements suggest that the Mn^{2+} ions did not incorporate significantly into the initial precursor cluster, which accounts for the lack of Mn^{2+} emission in the cluster and the nanoparticles at the early stages of the reaction. The ESR signal on the Mn^{2+}-doped ZnSe nanoparticles, like that of other Mn^{2+}-doped II−IV nanoparticles, indicated the presence of two different Mn^{2+} sites in the lattice. One was the Mn^{2+} substituting into the tetrahedral Zn^{2+} lattice site. The other was the anomalous surface/interior defect site. The XAFS data support the assignment of two Mn^{2+} sites, one being the substituted Zn^{2+} site and the other a surface Mn^{2+} site with additional O and or N neighbors, which possibly created an octahedral environment for the Mn^{2+} ions. This surface Mn^{2+} acts to quench the ZnSe luminescence but gives no Mn^{2+} emission.

Experimental Section

Synthesis of Mn^{2+}-Doped ZnSe Nanoparticles. All chemicals were acquired from Alfa-Aesar or Aldrich and were used without further purification. The synthetic method used was a modification of that developed by Cumberland et al.[37] $(Me_4N)_4[Zn_{10}Se_4(SPh)_{16}]:Mn^{2+}{}_x$ molecular clusters were prepared following the procedure of Dance et al.[40] A 6.3462 g amount of $(Me_4N)_2[Zn_4(SPh)_{10}]$, 0.6734 g of Se powder, and varying amounts of manganese acetate were dissolved in 50 mL of *N*,*N*-dimethylformamide (DMF). Three different $(Me_4N)_4[Zn_{10}Se_4(SPh)_{16}]:Mn^{2+}{}_x$ molecular clusters were prepared, each with a different amount of manganese acetate. Samples A, B, and C had 0.0228 (∼0.6%), 0.2857 (∼6%), and 2.1675 g (∼37%) of manganese acetate, respectively. The solution was allowed to sit for several minutes. Then, it was filtered to remove any unreacted Se. Approximately 0.6 g of the $(Me_4N)_4[Zn_{10}Se_4(SPh)_{16}]:Mn^{2+}{}_x$ cluster was added to 80 mL of hot HDA, which had been previously kept under vacuum at 120 °C for 2 h. Once the clusters had dissolved, the temperature was raised slowly to 280 °C. Particle growth was monitored by UV−vis and luminescence spectroscopy, and the temperature was modulated between 200 and 280 °C to control the rate of particle growth. When the desired particle size was achieved, as determined by UV−vis spectroscopy, the particles were annealed at 180 °C overnight.

To extract the particles from solution, the reaction solution was cooled to 80 °C and then poured into 100 mL of methanol, immediately forming a white precipitate. The mixture was centrifuged, and the methanol was discarded. The remaining white powder was dissolved in toluene. Additionally, the nanoparticle solution was filtered, and the toluene was evaporated. The nanoparticle powder was then washed with warm dry methanol, dissolved in heptane, and filtered. All of the nanoparticles were grown to the same size as determined by UV−vis. Undoped ZnSe nanoparticles were also prepared by following the method of Cumberland et al.[37]

XAFS of Mn^{2+}-Doped ZnSe Nanoparticles. XAFS data were taken at the Stanford Synchrotron Radiation Laboratory (SSRL) on beam line 4-3 using a Si 220 monochromator. The samples used for XAFS were prepared by adsorbing a toluene solution of the Mn^{2+}-doped ZnSe nanoparticle onto filter paper and uniformly dispersing a fine powder of the $(Me_4N)_4[Zn_{10}Se_4(SPh)_{16}]:Mn^{2+}{}_x$ cluster onto Scotch Tape. A sample of bulk ZnSe was also prepared by dispersing a fine powder of this material onto Scotch Tape. Fluorescence data were taken at the Mn K-edge, and transmission data were collected at the Zn K-edge and Se K-edge. All measurements were taken at 20 K. The fluorescence data were reduced by fitting the pre- and postedge backgrounds to a line with a constant baseline and a spline function, respectively, while the transmission data were reduced by fitting the pre- and postedge background to a Victoreen function and a spline function, respectively. The XAFS were then Fourier transformed and fitted in real space using RSFIT with standards generated by FEFF7.[41−43] A 3.5−9 $Å^{-1}$ Fourier transform range was used for the analysis of Mn edge data while a 3.5−13.5 $Å^{-1}$ Fourier transform range was used for the analysis of the Zn and Se edge data, except for the Zn K-edge data for the data for sample C, where the range was 3.5−12.5 $Å^{-1}$.

ESR of Mn^{2+}-Doped ZnSe Nanoparticles. The X-Band (9.43 GHz) ESR spectra were collected using a Bruker ESP380 ESR spectrometer and a TE_{102} cavity equipped with a variable temperature controller. The modulation amplitude was 10.6 G, and the microwave power was 26 mW. The data were collected for nanoparticles in toluene at 85 K.

Results

The UV−vis and luminescence spectra of a reaction mixture used to prepare sample B are presented in Figure 1. Initially, the reaction solution absorbs strongly in the blue with no sharp absorption bands at wavelengths greater than 350 nm. The corresponding luminescence spectrum with 340 nm excitation has a weak emission band with a maximum intensity at 441 nm and no Mn^{2+} emission. Over time, a sharp absorption band appears around 380 nm, and the corresponding luminescence spectrum showed signs of characteristic Mn^{2+} emission near 580 nm. As the temperature was increased, there was an increase in Mn^{2+} emission intensity and a red shift in the absorption band over time, which is an indication of particle growth. In the final stages of the reaction, ZnSe band edge emission at 415 nm becomes more prominent.

The sharp exciton absorption peak centered at 395 nm in the UV−vis spectrum of the final product in toluene is an indication

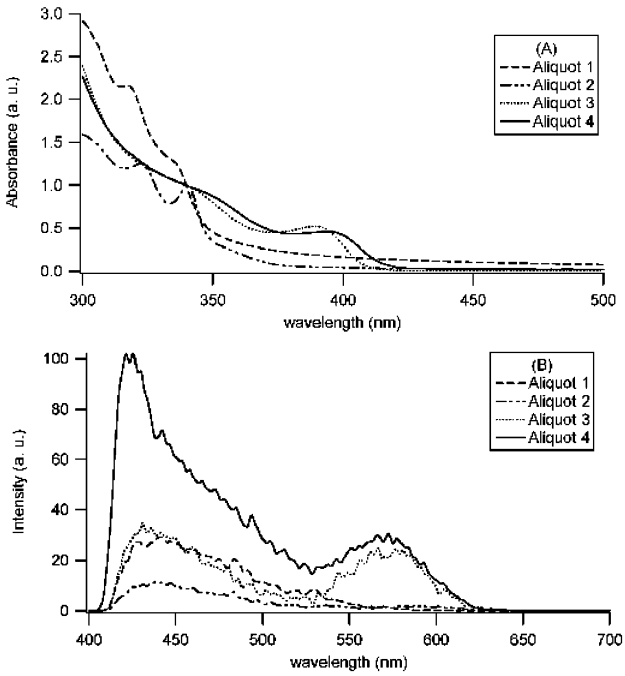

Figure 1. (A) Normalized UV−vis absorption spectra of Mn^{2+}-doped ZnSe nanoparticles B taken at different times in the reaction. Aliquot 1 was taken after the sample sat in the reaction solution for 2 h at 120 °C, aliquot 2 was taken after the sample sat at 180 °C for 14 h, and aliquots 3 and 4 were take consecutively during the growth of the nanoparticle in the 240−280 °C temperature range. (B) The corresponding emission spectrum of Mn^{2+}-doped ZnSe nanoparticles taken from the reaction. The excitation wavelength was 340 nm.

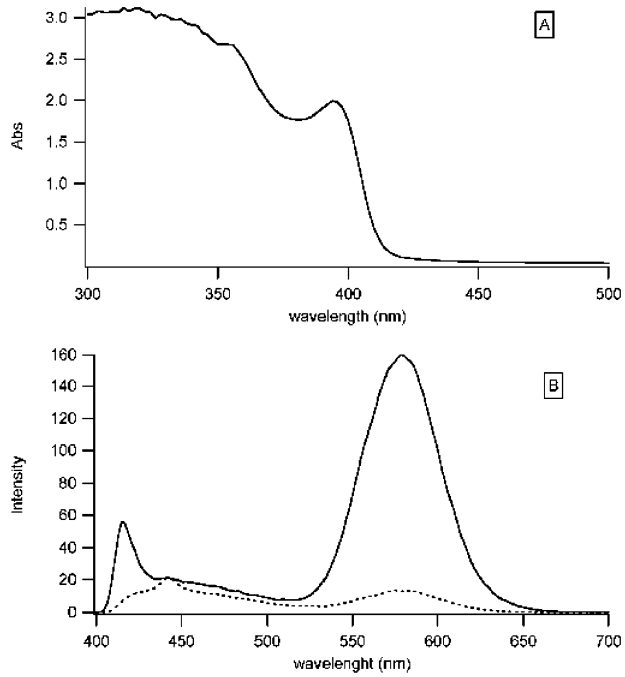

Figure 2. (A) UV−vis spectrum of Mn^{2+}-doped ZnSe nanoparticles (sample B) in toluene. (B) The emission spectrum of Mn^{2+}-doped ZnSe nanoparticles (sample B). The excitation wavelength was 390 nm. The solid line is the emission of a fresh sample, and the dotted dashed line is the emission of an aged sample.

that monodisperse particles were produced (Figure 2A). The position of the absorption maximum for the exciton peak suggests that the average particle diameter for the Mn^{2+}-doped ZnSe nanoparticles is 3.5 nm.[36] Transmission electron microscopy (TEM) data support this size assignment (Figure 3). For

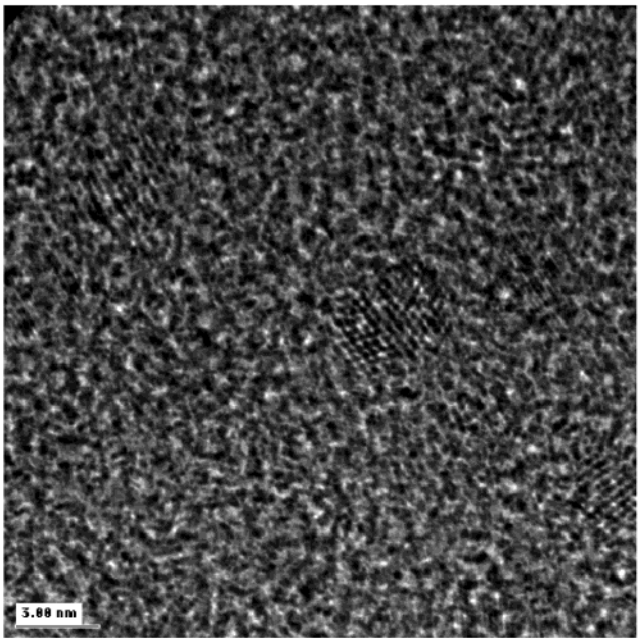

Figure 3. HRTEM micrograph of Mn^{2+}-doped ZnSe nanoparticles from sample B.

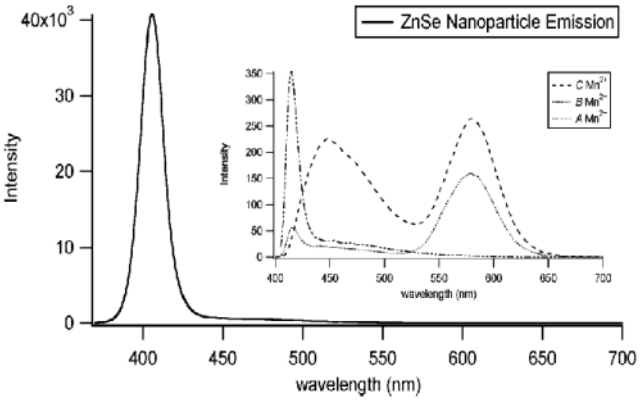

Figure 4. Comparison of the luminescence spectrum of undoped ZnSe nanoparticles and Mn^{2+}-doped ZnSe nanoparticles samples A, B, and C. The excitation wavelength was 357 nm for the undoped ZnSe and 390 nm for the doped nanoparticles.

particles of this size, approximately one-quarter of the atoms will be on the surface of the nanoparticle.

The luminescence spectrum with 390 nm excitation shows three distinct emission bands (Figure 2B) centered at 415, 441, and 580 nm, respectively. These bands can be assigned to ZnSe band edge, trap state, and Mn^{2+} $^4T_1 \rightarrow {}^6A_1$ emission. After aging for several days in the toluene solution, there was an overall drop in emission with significant decreases in the ZnSe band edge and Mn^{2+} $^4T_1 \rightarrow {}^6A_1$ emission.

The manganese concentration had an effect on the luminescence characteristics of the nanoparticles (Figure 4). In the doped samples, there was a slight red shift in the ZnSe band edge emission peak position and a significant decrease in ZnSe band edge emission intensity as compared to the undoped ZnSe sample, which had a quantum yield of ∼2% relative to perylene. Sample A had no Mn^{2+} $^4T_1 \rightarrow {}^6A_1$ emission but a substantial amount of ZnSe band edge emission and trap state emission. B had Mn^{2+} $^4T_1 \rightarrow {}^6A_1$ emission and a reduction of ZnSe band edge and trap state emission. C showed an increase in Mn^{2+} emission intensity as compared to B and an increase in trap state emission. The trap state emission had a maximum intensity

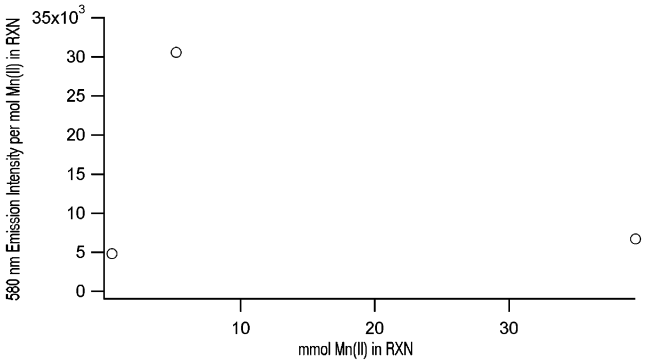

Figure 5. Plot of the 580 nm emission per Mn^{2+} ion vs the mmol Mn^{2+} used in the reaction. Qualitatively, this is an indication of Mn^{2+} quenching of the luminescence.

comparable to that of the Mn^{2+} emission. When the 580 nm emission intensity per Mn^{2+} ion was plotted vs the mmol of Mn^{2+} ion used in the reaction (Figure 5), it becomes apparent that in actuality the Mn^{2+} emission is quenched as the Mn^{2+} level is increased between B and C. This trend should be viewed qualitatively since the actual concentration of Mn^{2+} in the nanoparticles was not known. Suyver et al.[35] observed a similar trend in emission from their Mn^{2+}-doped ZnSe samples. Interestingly, in sample A, the reduction in ZnSe band edge emission as compared to the undoped sample suggests that little Mn^{2+} is needed to quench ZnSe band edge emission.

The local environment of the Mn^{2+} ion in the nanoparticles and precursor clusters was probed using XAFS and ESR. The ESR signal of the Mn^{2+}-doped ZnSe nanoparticle B (Figure 6A) showed the classic six-line hyperfine splitting pattern of Mn^{2+}. The hyperfine coupling constant was 61.87×10^{-4} cm^{-1}, which is consistent with reported values for Mn^{2+}-doped ZnSe in nanoparticles and bulk material.[36] However, superimposed upon this pattern is another six-line splitting pattern with a hyperfine coupling constant of 63.30×10^{-4} cm^{-1}, which, in Mn^{2+}-doped ZnS, has been attributed to Mn^{2+} at interstitial or surface sites of octahedral geometry in the nanoparticle lattice.[25] The slight broadening of the ESR spectrum suggests that exchange coupling may be occurring in this sample. The broadening was more pronounced in sample C (Figure 6B), which suggests that stronger exchange interactions are occurring. Sample A had no ESR signal. The ESR signal for the corresponding $(Me_4N)_4[Zn_{10}Se_4(SPh)_{16}]$:$Mn^{2+}$ clusters showed only a broad resonance (Figure 6C).

The XAFS data for the Mn^{2+}-doped ZnSe nanoparticle are presented in Figure 7 and Table 1. The XAFS parameters, position (R), Debye−Waller Factor (σ), which is a measure of the level of disorder in the system, and amplitude for the first and second peak were determined by fitting the data over an R range of 1.3−2.3, and 3.3−4.3 Å, respectively. For the Zn K-edge data, the best fit was achieved by treating the first peak as a combination of a Zn−Se and Zn−O coordination shell with an amplitude ration for the two shells of 3:1. After an initial fit, the amplitudes for the two shells were fixed to 2.46 for the Zn−Se shell and 0.82 for the Zn−O shell. σ for the two shells was allowed to vary as was R. Likewise, the second peak was treated as a combination of two Zn−Zn coordination shells. R for the two shells was kept the same, but σ was allowed to vary. The amplitudes for the two shells were allowed to vary under the constraint that their sum equal 8. The Se K-edge and Mn K-edge data were fitted in a similar fashion, except no Se−O shell was used to fit the Se K-edge data. Also, the sum of the amplitudes of the Mn−Se and Mn−O shells in the Mn K-edge

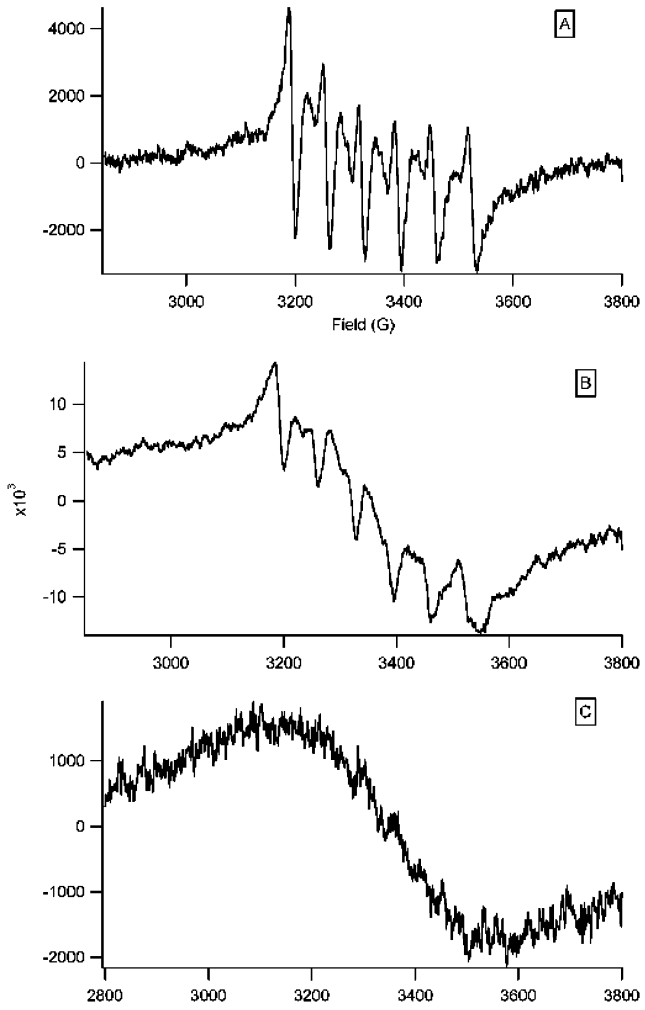

Figure 6. (A) ESR spectrum of Mn^{2+}-doped ZnSe nanoparticles B. The g value is 2.0179 ± 0.0004, and hyperfine coupling constants are 61.87×10^{-4} and 63.30×10^{-4} cm^{-1}. (B) The ESR spectrum of Mn^{2+}-doped ZnSe nanoparticles C. (C) The ESR spectrum of Mn precursor cluster. The g value is 2.0136 ± 0.0001.

data was fixed to 4, and the amplitudes were allowed to vary under this constraint. Because of the similarities between the theoretical models used to fit the data, no distinguishable Zn−Mn or Mn−Mn shell could be identified. The number of atoms in the different coordination shells was calculated using the equation

$$N = A/S_0^2$$

where N is the number of atoms, A is the measured amplitude, and S_0^2 is the amplitude reduction factor. The values for S_0^2 used to calculate N for the Zn K-edge and Se K-edge data were determined from the XAFS of bulk ZnSe. The value for S_0^2 for the Zn K-edge data was 0.81 and for Se K-edge was 0.93. A literature value of 0.82 for S_0^2 was used to calculate N for the Mn K-edge data.[18]

A comparison of the fitted XAFS parameters for samples A, B, and C does not reveal any strong trends that could be the effect of an increased Mn^{2+} concentration; however, there are some subtle differences in the Mn K-edge data. The Zn−Se distance is the same as bulk, as are the Zn−Zn and Se−Se distances. Interestingly, the Mn−Se distance is shorter than that of bulk Mn^{2+}-doped ZnSe as is the Mn−Zn distance.[44] The necessity to fit the second shell data with two N−N shells suggests that there are two types of second neighbors in

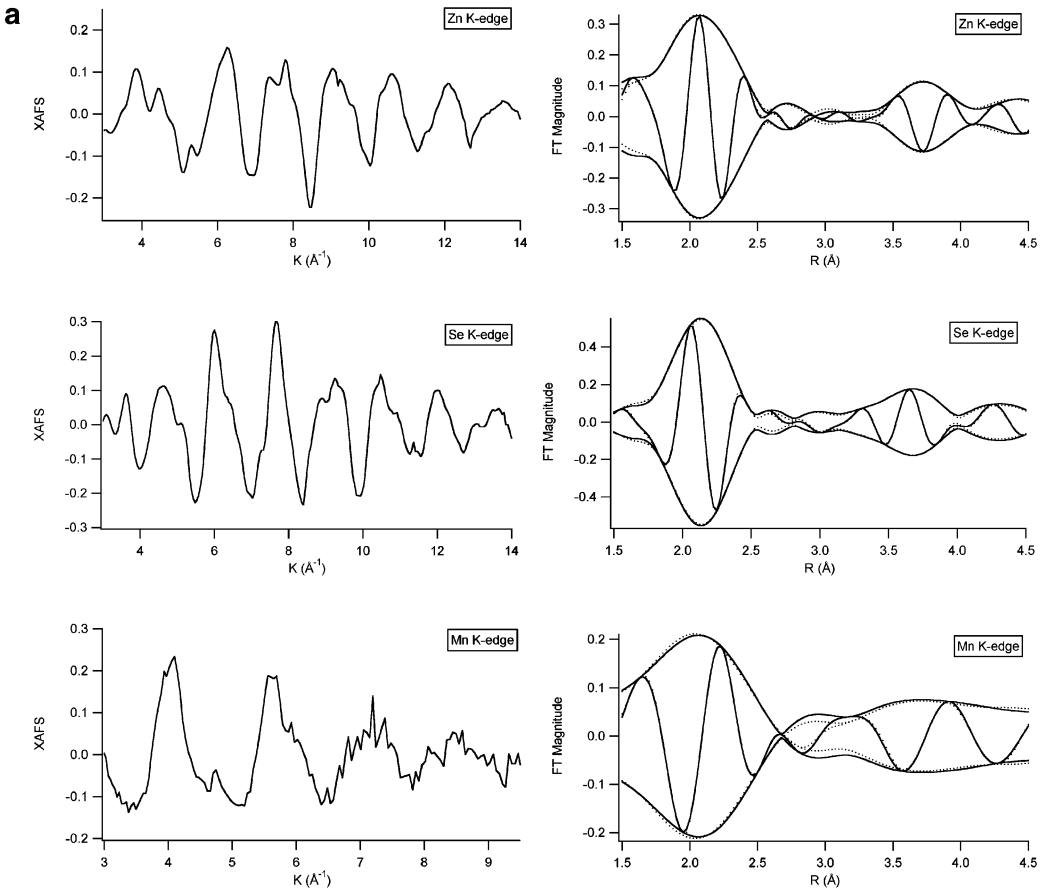
a
Zn K-edge
Se K-edge
Mn K-edge
XAFS
K (Å^{-1})
FT Magnitude
R (Å)

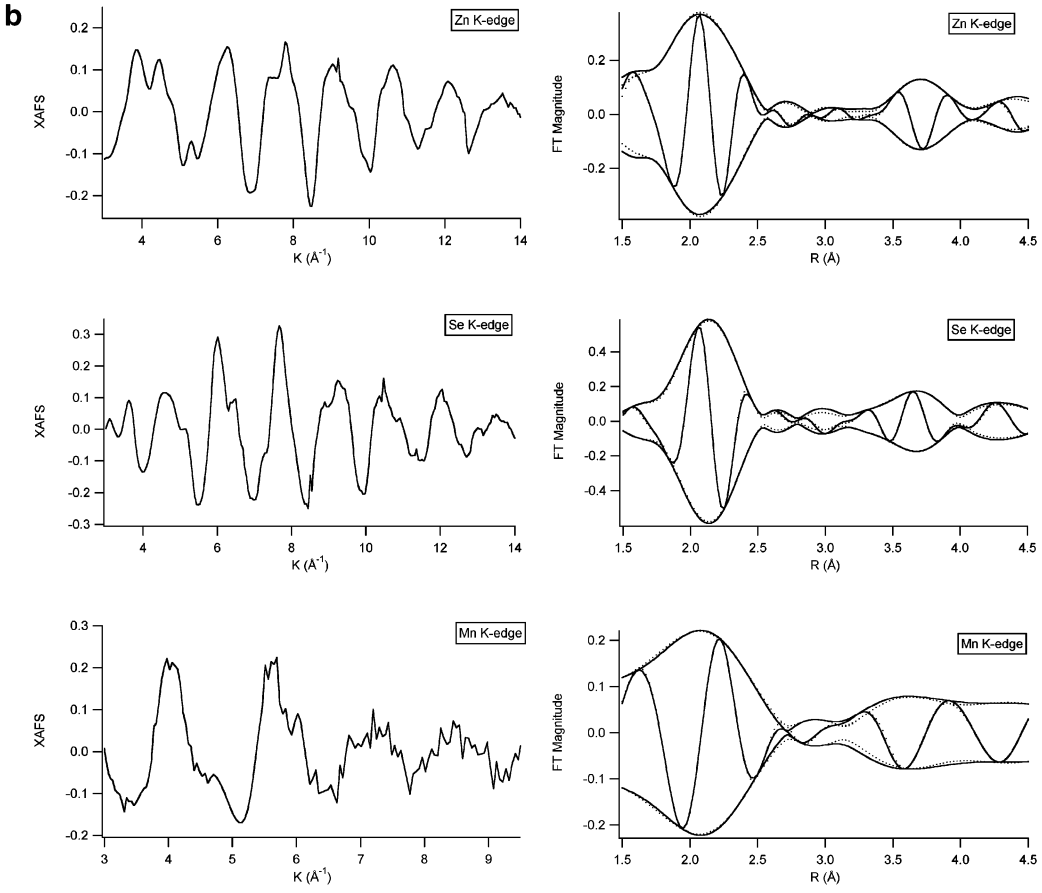
b
Zn K-edge
Se K-edge
Mn K-edge
XAFS
K (Å^{-1})
FT Magnitude
R (Å)

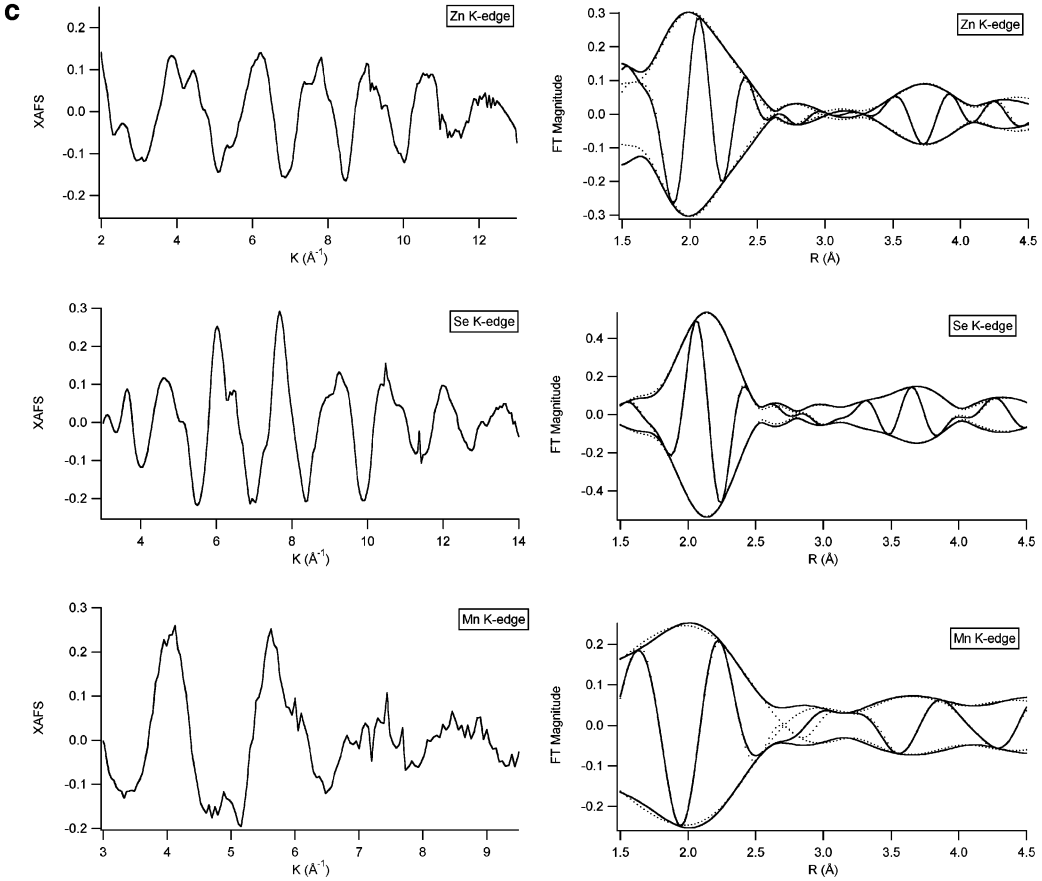

Figure 7. XAFS and FT-XAFS traces for (a) Mn^{2+}-doped ZnSe nanoparticles A, (b) Mn^{2+}-doped ZnSe nanoparticles B, and (c) Mn^{2+}-doped ZnSe nanoparticles C. The Fourier transform range is 3−14 Å^{-1} for the Zn K-edge and Se K-edge data, except for the Zn K-edge data in c, which had a Fourier transform range of 3−13 Å^{-1} and 3−9.5 Å^{-1} for the Mn K-edge. The XAFS data were collected at 20 K.

nanoparticles, with one type being more disordered than the other. In the Zn and Se K-edge data, the amount of disorder in these shells does not change with increasing Mn^{2+} concentration, but in the Mn K-edge data, sample C, the high Mn^{2+} concentration sample, has the lowest level of disorder for these shells. The necessity to fit the Zn and Mn K-edge data with a metal−O shell, and the lack of such a shell in the Se K-edge data, suggest that the surface of the particle is composed primarily of Zn and Mn ions. Furthermore, the decline in Mn−Se coordination number with increasing Mn^{2+} and the Mn−Se coordination being smaller than the Mn−O coordination suggest that most of the Mn^{2+} ions lie close to the surface of the nanoparticle. The large Mn−O coordination number also suggests that there could be Mn^{2+} atoms on the surface with octahedral geometry.

It is not apparent from the Mn K-edge XAFS of the precursor that there is any Mn^{2+} incorporation into it (Figure 8). Although the second shell is suggestive of metal−metal coordination, Mn substitution into a Zn site of $(Me_4N)_4[Zn_{10}Se_4(SPh)_{16}]$ cluster is not an accurate model of the data, since the first shell peak is more characteristic of a Mn−O shell than Mn−Se. The XAFS data for the precursor are best fit to a model that consists of a Mn cluster with O and Se coordination. Thus, the XAFS data in Figure 7 probably reflex the presence of Mn in different coordination environments from Mn acetate to a Mn DMF cluster or even a $(Me_4N)_4Zn_{10-x}Mn_xSe_4(SPh)_{16}$ cluster.

Discussion

The results suggest that the thermal decomposition of $(Me_4N)_4[Zn_{10}Se_4(SPh)_{16}]$:$Mn^{2+}{}_x$ in HDA led to the formation of Mn^{2+}-doped ZnSe nanoparticles. The lack of Mn^{2+} emission in the early stages of the reaction and the Mn K-edge XAFS of the cluster (Figure 8) indicate that there was no significant Mn^{2+} incorporation into the $(Me_4N)_4[Zn_{10}Se_4(SPh)_{16}]$ cluster, although some type of Mn^{2+} species coexisted with this compound. Incorporation into the particle must have occurred during nanoparticle growth. This is consistent with the model for nanoparticle growth proposed by Cumberland et al.[37] During the reaction, $(Me_4N)_4[Zn_{10}Se_4(SPh)_{16}]$ reduces to a $[Zn_6Se_4]_n$ cluster into which the Mn^{2+} ions incorporated during nanoparticle formation. The emergence of Mn^{2+} emission does not appear to be a size-dependent phenomenon, since the Mn^{2+} emission emerged over time with only a negligible shift in the UV−vis spectrum, which is a function of particle size.

The presence of the Mn^{2+} $^4T_1 \rightarrow {}^6A_1$ emission peak and the quenching of the ZnSe band edge emission were clear signs of Mn^{2+} incorporation into the nanoparticles. The dependence of the emission intensity on Mn^{2+} concentration is expected;[35] however, the dramatic increase in trap state emission from sample B to C was somewhat surprising. The decline in overall sample emission intensity over time is most likely due to the presence of H_2O or some other species adsorbed onto the particles surface. Water is known to quench nanoparticle luminescence,[45] and when the nanoparticles were extracted from HDA using dry solvents, the samples remained emissive for a longer period of time. A surface species or adsorbate, which disrupts the surface by introducing new surface states, might also explain enhanced trap state emission of sample C.

A 3.5 nm particle size determined by UV−vis and TEM was used in constructing a structural model for the nanoparticles. ZnSe nanoparticles prefer the Zinc Blende structure,[34] and bulk

TABLE 1: Table of the Measured XAFS Parameters Determined from Fitting the XAFS Data in Real Space[a]

	A	B	C	bulk
Zn K-edge parameters				
Zn−Se distance (Å)	2.44	2.44	2.43	2.45
Zn−Se coordination number	3.04	3.04	3.04	4
σ Zn−Se (Å)	0.055	0.048	0.061	0.050
Zn−Zn distance (Å)	4.01	3.99	3.98	4.01
Zn−Zn coordination number	4.64	4.81	3.93	12
σ Zn−Zn (Å)	0.076	0.071	0.079	0.068
Zn−Zn′ coordination number	5.24	5.06	5.95	
σ Zn−Zn′ (Å)	0.104	0.127	0.128	
Zn−O (N) distance (Å)	2.18	2.11	2.22	2.14
Zn−O (N) coordination number	1.01	1.01	1.01	
σ Zn−O (N) (Å)	0.061	0.047	0.057	
Se K-edge parameters				
Se−Zn distance (Å)	2.45	2.45	2.45	2.45
Se−Zn coordination number	3.99	3.99	3.99	4
σ Se−Zn (Å)	0.053	0.049	0.055	0.050
Se−Se distance (Å)	3.94	3.91	3.92	4.00
Se−Se coordination number	5.54	3.42	4.27	12
σSe−Se (Å)	0.084	0.068	0.076	0.064
Se−Se′ coordination number	4.14	6.25	5.45	
σSe−Se′ (Å)	0.088	0.107	0.095	
Mn K-edge parameters				
Mn−Se distance (Å)	2.42	2.43	2.44	2.54
Mn−Se coordination number	1.90	1.96	1.45	4
σ Mn−Se (Å)	0.088	0.071	0.054	
Mn−Zn distance (Å)	4.07	4.07	4.04	4.06
Mn−Zn coordination number	2.21	2.26	4.15	12
σ Mn−Zn (Å)	0.078	0.068	0.076	
Mn−Zn′ coordination number	7.55	7.50	5.60	
σ Mn−Zn′ (Å)	0.113	0.113	0.083	
Mn−O (N) distance (Å)	2.26	2.22	2.22	2.22
Mn−O (N) coordination number	2.98	2.91	3.44	
σ Mn−O (N) (Å)	0.073	0.051	0.033	

[a] The bulk values listed in the Zn K-edge and Se K-edge data set are those of the measured bulk ZnSe. The bulk values for the distance in the Mn K-edge data set were those of $Zn_{0.85}Mn_{0.15}Se$ reported in ref 44, and the coordination numbers were those of the theoretical standard as was the Mn−O distance. The Zn−O distances were calculated from ionic radii of Zn and O.

ZnSe has a lattice constant of 5.6686 Å. Thus, a particle of 3.5 nm would have ∼10 coordination shells centered around a central atom, which in our model was Zn. The number of atoms in each coordination shell was calculated using the difference of the equations

$$S_n = 1/12\ (10n^3 + 15n^2 + 26n + 12) \text{ for even values of } n$$

$$S_n = 1/12\ (10n^3 + 15n^2 + 26n + 9) \text{ for odd values of } n$$

where n is the number of coordination shells and S_n is the number of atoms of clusters of n shells.[46] This model yields a nanoparticle composed of 981 atoms with ∼26% of them occupying the particles surface. On the basis of this model, the average first neighbor coordination is ∼3.22 atoms and the second neighbor coordination is ∼9.65 atoms; however, the true average first and second neighbor coordination will be dependent upon the particle morphology.[47] These coordination numbers were used as guides to fit the XAFS data. The initial fits produced Zn second coordination in the Zn and Mn K-edge data that was significantly lower than expected and were not consistent with this model. The initial fits of the Se K-edge data produced Se−Se second shell coordination that was higher than expected, which suggests that the environment around the Se atoms was similar to bulk ZnSe. However, to get coordination numbers that were consistent with the model, an additional second neighbor shell was incorporated into the fit. The Zn−Zn′, Mn−Zn′, and Se−Se′ shells introduced into the fit brought the total second shell coordination value to close to what was expected, but these shells have a larger σ than their counterparts. From these data, we propose that the surface of the nanoparticle is more disordered than the particle interior.

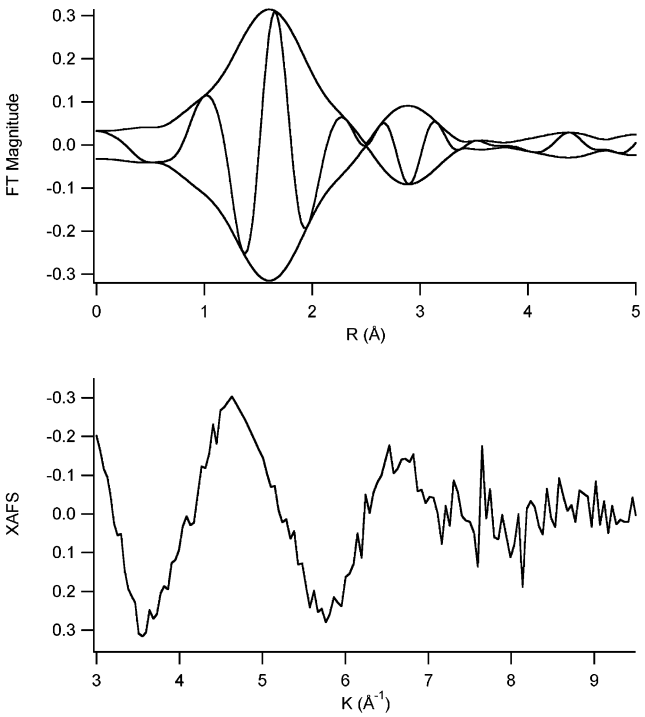

Figure 8. XAFS and FT-XAFS traces taken at the Mn K-edge of $(Me_4N)_4[Zn_{10}Se_4(SPh)_{16}]:Mn^{2+}$. The XAFS data were collected at 20 K. Note that the first peak is shifted to lower R and is consistent with the peak positions of Mn−O in MnO.

The XAFS and ESR data suggest that the Mn^{2+} in the nanoparticles occupies two sites in the ZnSe lattice. One site is an interior Zn site, and the other is possibly a surface site of octahedral geometry. The ESR signal from the nanoparticles has three distinct features: (i) a six-line hyperfine splitting pattern due to Mn^{2+} substituting for a Zn^{2+} ion in the lattice, (ii) exchange interaction, and (iii) a six-line splitting pattern due to Mn^{2+} occupation of a site other than the Zn^{2+} lattice site. This splitting pattern has been observed in other Mn^{2+}-doped II−VI nanoparticles, and this second Mn^{2+} site has been attributed to Mn surface or interstitial site of octahedral symmetry.[25,32] The Mn K-edge XAFS (Figure 7) suggests that a significant number of the Mn^{2+} ions in the nanoparticles occupy the Zn^{2+} site in the lattice, since the first and second neighbor coordination shell can be fit to a model of Mn^{2+} in the Zn^{2+} lattice site. However, the Mn^{2+} ions lack a full first shell coordination of Se, which is an indication of the presence of Mn^{2+} on the surface of the nanoparticles. The Mn−Se shell coordination number is smaller than the Zn−Se shell coordination number, indicating that a significant portion of the Mn^{2+} ions occupy a region close to the particles surface. An Mn−O first coordination shell was added to better fit the data; however, because O and N are similar in atomic number, this shell could be a metal−N shell resulting from the coordination of HDA to the nanoparticle surface. The sum of the Mn−Se and Mn−O coordination number gives a slightly larger first neighbor coordination number than expected for Mn^{2+} in a tetrahedral environment. This would suggest that the surface Mn^{2+} has a different geometry than that of the interior. Because physically it is likely that only one HDA molecule bonds to one surface

metal atom of the nanoparticle, the additional atoms modeled most likely belong to an oxygen species such as OH^- or O^{2-}. Mn^{2+} in MnO has octahedral geometry, and the Mn−O bond distance determined from the fitting is consistent with that of Mn−O. Thus, the surface Mn most likely possesses octahedral geometry, due to the additional O coordination, while the interior Mn is of tetrahedral geometry. This interpretation of the XAFS data complements the inference of a surface octahedral site from the ESR data. The Mn−O coordination observed in the XAFS helped to create the octahedral environment observed in the ESR. Similar to the Mn data, a Zn−O shell was also included in the fit, giving it a full first neighbor coordination shell to the Zn atoms. The additional first coordination shell for the Zn K-edge data is an indication of HDA and or OH^-/O^{2-} coordination to the particles surface.

These structural factors can be used to explain some of the luminescence behavior of the nanoparticles studied. In the reaction to form the nanoparticles, the Mn^{2+} emission occurs late in the reaction and only for reaction solutions B and C. The addition of a small amount of Mn^{2+} to the ZnSe nanoparticles, as was the case in sample A, had the effect of quenching the ZnSe band edge emission. Along with the XAFS and ESR data, which identified distinct Mn^{2+} surface and interior sites, the late emergence of Mn^{2+} emission from the reaction solution suggests that there is not a uniform or homogeneous distribution of Mn^{2+} in the nanoparticles. It is likely that the surface Mn^{2+} lacks the Mn^{2+} $^4T_1 \rightarrow {}^6A_1$ emission, possesses octahedral geometry, and acts as a quencher for both ZnSe band edge and Mn^{2+} emission. Consequently, in sample A, the surface Mn^{2+} may have formed preferentially over the interior Mn^{2+}. Thus, only ZnSe band edge quenching was observed in that sample and no Mn^{2+} emission was observed. In sample B, more Mn^{2+} was present in the reaction solution; therefore, more Mn^{2+} incorporated into the interior, and $^4T_1 \rightarrow {}^6A_1$ emission occurs along with a further quenching of the ZnSe band edge emission. Sample C, which had the most Mn^{2+} present in the reaction solution, showed essentially no ZnSe band edge emission but strong trap state emission and Mn^{2+} emission. In terms of Mn^{2+} emission per mmol Mn^{2+}, C possessed less Mn^{2+} emission than B, indicating that quenching from either surface Mn^{2+} or Mn^{2+}−Mn^{2+} mers was occurring. The presence of a large number of octahedral surface Mn^{2+} could have the effect of distorting the lattice on the surface of the nanoparticles, thus increasing the number of surface trap states. Also, the additional water bound to the octahedral surface Mn^{2+} could act as an electron or hole trap in a fashion similar to the matrix quenching effects observed in some nanoparticle systems.[48,49] The presence of surface OH^-/O^{2-} species can also have the effect of quenching the luminescence in nanoparticles.[45] These surface bound OH^-/O^{2-} may account for the decline in emission over time and the reduction in the overall luminescence quantum efficiency of the nanoparticles. Thus, it is likely that the octahedral surface Mn^{2+} acts solely as a luminescence quencher, and the interior Mn^{2+} is the Mn^{2+} $^4T_1 \rightarrow {}^6A_1$ emission center that also quenches the ZnSe band edge emission.

Conclusion

Mn^{2+}-doped ZnSe was synthesized from the thermal decomposition of ZnSe molecular clusters in the presence of Mn^{2+} ions in a coordinating solvent. A uniform and homogeneous distribution of Mn^{2+} in the nanoparticle was not achieved; consequently, the Mn^{2+} ions lie toward the surface of the nanoparticles and possibly occupy two different sites in the nanoparticle lattice. One site is the Zn tetrahedral site, and the other is likely an octahedral surface site. It is the interior Mn^{2+} that is the $^4T_1 \rightarrow {}^6A_1$ emission center while the surface site acts solely as a luminescence quencher. The results suggest that the local structure and environment of the Mn^{2+} ions have a significant influence on the optical properties of Mn^{2+}-doped semiconductor nanomaterials.

Acknowledgment. We thank Prof. Geoffrey Strouse and Dr. Stephen Woessner for their many helpful suggestions and advice on nanoparticle synthesis. We also thank Prof. Stanley Williamson, Prof. Rebecca Braslau, Aaron Nilsen, Chris Grant, Lisa Downwood, Ryan Baumbach, Shawna Bushant, and Chris Nelson for their assistance. This project was supported by grants from MBRS/NIH GM58903, Department of Education, GAANN, UC LEADS, the DOE at SSRL, National Center for Electron Microscopy, the Petroleum Research Fund administered by the American Chemical Society, the Collaborative UC/Los Alamos National Labs (CULAR), the Materials Research Institute of Lawrence Livermore National Labs, and the Campus (UC)/Labs (LLNL) exchange program.

References and Notes

(1) Wang, Y. *Acc. Chem. Res.* **1991**, *24*, 133.
(2) Henglein, A. *Chem. Rev.* **1989**, *89*, 1861.
(3) Efros, A. L. *Sov. Phys. Semicond.* **1982**, *16*, 772.
(4) Brus, L. E. *J. Chem. Phys.* **1984**, *80*, 4403.
(5) Tolbert, S. H.; Alivisatos, A. P. *Annu. Rev. Phys. Chem.* **1995**, *46*, 595.
(6) Fendler, J. H.; Meldrum, F. C. *Adv. Mater.* **1995**, *7*, 607.
(7) Alivisatos, A. P. *J. Chem. Phys.* **1996**, *100*, 13226.
(8) Alivisatos, A. P. *Science* **1996**, *271*, 933.
(9) Liu, J.; Feng, X. D.; Fryxell, G. E.; Wang, L. Q.; Kim, A. Y.; Gong, M. L. *Adv. Mater.* **1998**, *10*, 161.
(10) Kamat, P. V. *Prog. Inorg. Chem.* **1997**, *44*, 273.
(11) Zhang, J. Z. *Acc. Chem. Res.* **1997**, *30*, 423.
(12) Collier, C. P.; Vossmeyer, T.; Heath, J. R. *Annu. Rev. Phys. Chem.* **1998**, *49*, 371.
(13) Heath, J. R.; Shiang, J. J. *Chem. Soc. Rev.* **1998**, *27*, 65.
(14) O'Regan, B.; Gratzel, M. *Nature* **1991**, *353*, 737.
(15) Chen, W.; Joly, A. G.; Zhang, J. Z. *Phys. Rev. B* **2001**, *64*, 041202/041201−041204.
(16) Bol, A. A.; Meijerink, A. *Phys. Rev. B* **1998**, *58*, R15997−R16000.
(17) Jae Hun, C.; Chil Seong, A.; Du-Jeon, J. *J. Phys. Chem. B* **2001**, *105*, 4128−4132.
(18) Soo, Y. L.; Ming, Z. H.; Huang, S. W.; Kao, Y. H.; Bhargava, R. N.; Gallagher, D. *Phys. Rev. B* **1994**, *50*, 7602−7607.
(19) Qi, J.; Guo, X.; Sakurai, K.; Masumoto, Y. *Scr. Mater.* **2001**, *44*, 2315−2319.
(20) Dinsmore, A. D.; Hsu, D. S.; Qadri, S. B.; Cross, J. O.; Kennedy, T. A.; Gray, H. F.; Ratna, B. R. *J. Appl. Phys.* **2000**, *88*, 4985−4993.
(21) Dinsmore, A. D.; Hsu, D. S.; Gray, H. F.; Qadri, S. B.; Tian, Y.; Ratna, B. R. *Appl. Phys. Lett.* **1999**, *75*, 802−804.
(22) Jin, C.; Yu, J.; Sun, L.; Dou, K.; Hou, S.; Zhao, J.; Chen, Y.; Huang, S. *J. Lumin.* **1995**, *66*−*67*, 315−318.
(23) Smith, B. A.; Zhang, J. Z.; Joly, A.; Liu, J. *Phys. Rev. B* **2000**, *62*, 2021−2028.
(24) Bol, A. A.; Meijerink, A. *Phys. Status Solidi* **2001**, *224*, 291−296.
(25) Borse, P. H.; Srinivas, D.; Shinde, R. F.; Date, S. K.; Vogel, W.; Kulkarni, S. K. *Phys. Rev. B* **1999**, *60*, 8659−8664.
(26) Bhargava, R. N.; Gallagher, D.; Hong, X.; Nurmikko, A. *Phys. Rev. Lett.* **1994**, *72*, 416−419.
(27) Suyver, J. F.; Wuister, J. J.; Kelly, J. J.; Meijerink, A. *Nano Lett.* **2001**, *1*, 429.
(28) Khosravi, A. A.; Kundu, M.; Kuruvilla, B. A.; Shekhawat, G. S.; Gupta, R. P.; Sharma, A. K.; Vyas, P. D.; Kulkarni, S. K. *Appl. Phys. Lett.* **1995**, *67*, 2506−2508.
(29) Yu, J.; Liu, H.; Wang, Y.; Jia, W. *J. Lumin.* **1998**, *79*, 191.
(30) Igarashi, T.; Ihara, M.; Kusunoki, T.; Ohno, K.; Isobe, T.; Senna, M. *J. Nanopart. Res.* **2001**, *3*, 51−56.
(31) Hofmann, D. M.; Hofstaetter, A.; Leib, U.; Meyer, B. K.; Counio, G. *J. Cryst. Growth* **1998**, *184*/*185*, 383−387.
(32) Counio, G.; Esnouf, S.; Gacoin, T.; Boilot, J. P. *J. Chem. Phys.* **1996**, *100*, 20021.
(33) Mikulec, F. V.; Kuno, M.; Bennati, M.; Hall, D. A.; Griffin, R. G.; Bawendi, M. G. *J. Am. Chem. Soc.* **2000**, *122*, 2532.
(34) Hines, M. A.; Guyot-Sionnest, P. *J. Phys. Chem. B* **1998**, *102*, 3655−3657.

(35) Suyver, J. F.; Wuister, S. F.; Kelly, J. J.; Meijerink, A. *Phys. Chem. Chem. Phys.* **2000**, *2*, 5445.
(36) Norris, D. J.; Nan, Y.; Charnock, F. T.; Kennedy, T. A. *Nano Lett.* **2001**, *1*, 3−7.
(37) Cumberland, S. L.; Hanif, K. M.; Javier, A.; Khitrov, G. A.; Strouse, G. F.; Woessner, S. M.; Yun, C. S. *Chem. Mater.* **2002**, *14*, 1576−1584.
(38) Hanif, K. M.; Meulenberg, R. W.; Strouse, G. F. *J. Am. Chem. Soc.* **2002**, *124*, 11495−11502.
(39) Hagen, K. S.; Stephan, D. W.; Holm, R. H. *Inorg. Chem.* **1982**, *21*, 8−3936.
(40) Dance, I. G.; Choy, A.; Scudder, M. L. *J. Am. Chem. Soc.* **1984**, *106*, 5−6295.
(41) Liu, G. G.; Bridges, F.; Booth, C. H. *Phys. Rev. B* **1995**, *52*, 6332.
(42) Bridges, F.; Booth, C. H.; Liu, G. G. *Phys. B* **1995**, *208*−*209*, 121.
(43) Zabinsky, S. I.; Rehr, J. J.; Ankudinov, A.; Albers, R. C.; Eller, M. J. *Phys. Rev. B* **1995**, *52*, 2995.
(44) Pong, W. F.; Mayanovic, R. A.; Bunker, B. A.; Furdyna, J. K.; Debska, U. *Phys. Rev. B* **1990**, *41*, 8440−8448.
(45) Tata, M.; Banerjee, S.; John, V.; Waguespack, Y.; McPherson, G. L. *Colloid Surf. A* **1997**, *127*, 39.
(46) Hill, N. A.; Whaley, B. *J. Chem. Phys.* **1993**, *99*, 3707−3715.
(47) Fritsche, H. G.; Benfield, R. E. *Z. Phys. D* **1993**, *26*, S15−S17.
(48) Hess, B. C.; Okhrimenko, I. G.; Davis, R. C.; Stevens, B. C.; Schulzke, Q. A.; Wright, K. C.; Bass, C. D.; Evans, C. D.; Summers, S. L. *Phys. Rev. Lett.* **2001**, *86*, 3132−3135.
(49) Chen, W.; Joly, A.; Roark, J. *Phys. Rev. B* **2002**, *65*, 245404.